

THE EPOCH OF ASSEMBLY OF TWO GALAXY GROUPS: A COMPARATIVE STUDY

MATTHEW NICHOLS¹

Laboratoire d'Astrophysique, École Polytechnique Fédérale de Lausanne (EPFL), Observatoire de Sauverny, 1290 Versoix, Switzerland

AND

JOSS BLAND-HAWTHORN

Sydney Institute for Astronomy, School of Physics, The University of Sydney, NSW 2006, Australia

Draft version August 8, 2018

ABSTRACT

Nearby galaxy groups of comparable mass to the Local Group show global variations that reflect differences in their evolutionary history. Satellite galaxies in groups have higher levels of gas deficiency as the distance to their host decreases. The well established gas deficiency profile of the Local Group reflects an epoch of assembly starting at $z \lesssim 10$. We investigate whether this gas deficiency profile can be used to determine the epoch of assembly for other nearby groups. We choose the M81 group as this has the most complete inventory, both in terms of membership and multi wavelength observations. We expand our earlier evolutionary model of satellite dwarf galaxies to not only confirm this result for the Local Group but show that the more gas-rich M81 group is likely to have assembled at a later time ($z \lesssim 1 - 3$).

Subject headings: galaxies: dwarf — galaxies: interactions — galaxies: individual (M81) — Galaxy: evolution — Galaxy: halo — Local Group

1. INTRODUCTION

The predominant cosmological model of structure formation—dark energy and cold dark matter, Λ CDM—dictates that galaxy sized objects build up hierarchically through the merger of smaller structures. Throughout this build-up, these small structures are either destroyed, incorporated into the galaxy's halo, or become satellite subhalos of the host galaxy (Moore et al. 1999). The destroyed systems and those which survived to become satellites were likely similar, with the satellite subhalos becoming the modern day dwarf galaxies (Frebel et al. 2010).

That dwarf galaxies are likely relics of early galaxy formation has made them prominent targets for observational and theoretical studies of galactic formation. These include analysis of star formation thresholds (de Blok & Walter 2006; Ekta et al. 2008; Kuhlen et al. 2012), how the earliest galaxies formed (Ricotti et al. 2008; Tolstoy 2011; Frebel & Bromm 2012), the stellar yields of the first stars (Karlsson et al. 2012, 2013), the strength of reionization (Barkana & Loeb 1999; Somerville 2002; Hoefft et al. 2006; Sawala et al. 2012; Lunnan et al. 2012), and distinguishing between different forms of dark matter (Bode et al. 2001; Macciò & Fontanot 2010; Lovell et al. 2012). Satellite dwarfs may also be a guide to the accretion history of their host galaxy. With cosmological models showing large amounts of variation in the mass accretion history of galaxies (McBride et al. 2009; Boylan-Kolchin et al. 2010), variations in the redshifts at which satellite galaxies first fell in would be unsurprising.

Determining the accretion time of dwarf galaxies has involved either (i) calculating the orbits of dwarfs back-

wards in time (e.g. Besla et al. 2007; Lux et al. 2010; Bekki 2011) or (ii) statistical methods comparing infall epochs and the present day orbital properties of dwarf galaxies (Rocha et al. 2012; Teyssier et al. 2012). The accretion history of the Local Group can be derived by comparing the observed distance-HI deficiency relation in satellite galaxies (Grcevich & Putman 2009) with evolution models. A recent study has found that the Milky Way and M31 have been accreting satellites since $z \lesssim 10$ (Nichols & Bland-Hawthorn 2011, hereafter NBH).

Such a relation between the distance to the host and fraction of dwarfs that are deficient in HI is not unique to the Local Group, with other nearby groups showing a range of related trends (Karachentsev & Kaisin 2007; Rasmussen et al. 2012; Bahé et al. 2013; Crnojević et al. 2012; Roychowdhury et al. 2012; Chiboucas et al. 2013). We explore these trends to compare the likely differences in accretion history between these nearby groups. In order to achieve this, we use the model presented in NBH, but with an updated treatment of dwarf stripping to allow for the presence of disks and a larger subhalo mass range.

We use this new model to examine the accretion history of nearby galaxy groups based upon this distance/gas-deficiency relation to examine the relative mass accretion histories between the Local Group and the M81 group another nearby group. In §2, we present our improved dynamical model for an evolving galaxy group. In §3, we present the results of comparative study between the Local Group and the M81 group, and we present our conclusions in §4.

2. MODEL

To determine the final state of dwarf galaxies, a toy model of a dwarf galaxy is evolved on a random orbit from a redshift of $z = 10$. Here we describe the orbital model briefly before discussing the initial conditions of

matthew.nichols@epfl.ch

¹ Sydney Institute for Astronomy, School of Physics, The University of Sydney, NSW 2006, Australia

the dwarf, the heating and cooling of the gas and the stripping of the gas. Throughout the model we track 8 variables: four describing the galactocentric distance, angle of the dwarf and their derivatives, $(r, \theta, \dot{r}, \dot{\theta})$; R_d , the radial size of the dwarfs disk; M_d a parameter which describes the mass distribution of the dwarfs disk; R_h , the radial extent of the dwarfs hot halo and; X_c , the ratio of the cold gas mass in the disk to the total disk mass.

2.1. Orbital Model

For each run the dwarf galaxy has a random orbit determined by a phase, perigalacticon and circularity. The perigalacticon and circularity are selected by sampling the $z = 0$ infall distributions of Wetzel (2011) in an identical fashion to Nichols et al. (2011). We restrict the perigalacticon to a minimum value of 10 kpc. Dwarfs that end up closer in will have a much larger contribution from the disk of the Galaxy and will likely have been tidally destroyed. The distributions are assumed to continue past the virial radius to a maximum value of eight times the virial radius (~ 2 Mpc). Given the exponential nature of the distribution, this limit is likely to have minimal impact and is chosen only to avoid calculation of orbits wholly beyond the radius considered in the comparison. Dwarfs beyond the virial radius will never be considered to have infallen but do add a minor contribution to the fraction of gas deficient galaxies beyond the virial radius. The infall distribution with redshift is not constant. However, as the orbits would invariably change as the host halo grows (even ignoring dynamical friction) we assume the $z = 0$ distribution is representative of the final distribution of orbits.

A random phase is chosen by evolving the orbit from perigalacticon for 10 Gyr (an arbitrary amount of time) inside a static Einasto halo of mass equal to the model host galaxy at $z = 0$. A final position is then chosen by selecting the position at a random point in time up to the time of first apogalacticon (or 10 Gyr, whichever is later). Such a method accounts for the non-elliptical nature of orbits in an Einasto halo, while only missing a small fraction of the parameter space (the portion of the orbits that exceeds the age of the Universe). The dwarf is then randomly chosen to be heading towards or away from the host galaxy at $z = 0$.

The initial position (at $z = 10$) is then determined by evolving the final position backwards inside a growing Einasto potential where the equation of motions are given in NBH. The mass of the host galaxy is assumed to evolve according to the prescription given in Boylan-Kolchin et al. (2010)

$$M(z) = M_0(1+z)^{2.23} \exp[-4.90(\sqrt{1+z} - 1)]. \quad (1)$$

The profile of the host galaxy is assumed to be an Einasto profile with an Einasto parameter $\alpha = 0.16$ (for all mass ranges considered from dwarf galaxy to a few times the Milky Way, the parameter α is dominated by the constant term in fits to N -body simulations; Gao et al. 2008; Duffy et al. 2008). The concentration of the host halos is given by (Duffy et al. 2008)

$$c_{\text{vir}} = \frac{8.82}{(1+z)^{0.87}} \left(\frac{M_{\text{vir}}}{2 \times 10^{12} h M_{\odot}} \right)^{-0.106}. \quad (2)$$

The initial position is then used to evolve the orbit

forwards in time taking into account the evolution of the dwarf galaxy.

2.2. Dwarf Galaxy Initial Conditions

Dwarf galaxies are low mass, low luminosity galaxies with a broad array of morphologies. Despite the wide range of morphologies, it is likely that at least the majority of satellite dwarfs are examples of different evolutionary states of gas rich, disk containing “early-type” dwarfs (Mayer et al. 2001; Grebel et al. 2003; Pasetto et al. 2003; D’Onghia et al. 2009; Helmi et al. 2012). We hence model all dwarfs as if they originated from a constant template: a spherical dark matter halo containing a mixed warm/cold gas disk with a hot gas halo and the entire dwarf embedded inside a host galaxy halo filled with its own hot gas.

The dark matter halo of the dwarf galaxy is chosen to be a static Einasto profile with the mass a free parameter. An Einasto profile best matches the properties of dark matter halos arising through large N -body, dark matter simulations (Springel et al. 2008). All halos are modelled with an Einasto parameter of $\alpha = 0.16$ and a concentration at $z = 0$ of $c_{\text{dw},0} = 35$, the approximate median of dwarf galaxy sized halos in Colín et al. (2004). The choice of an Einasto profile is not without problems. Although the Einasto profile is the best match to dark matter simulations, observational results suggest that the central portion of dwarf galaxy dark matter halos may be constant density although this remains controversial with both “cored” and “cuspy” profiles seen (Simon et al. 2005; Del Popolo 2012; Wolf & Bullock 2012). Such a profile may arise through the halo consisting of warm dark matter rather than cold dark matter (Bode et al. 2001) or through baryonic processes such as non-adiabatic expulsion of gas from supernova (Pontzen & Governato 2012). We do not consider either situation in this paper, but we note that our method could be extended (with another free parameter) in principle to accommodate either case. The impact of the latter case is difficult to predict, since ram pressure stripping should remove gas reducing the star formation over time (and therefore the amount of supernova) such a process may result in the density profiles of dwarf galaxies being fundamentally different from host galaxy to host galaxy. This is a possibility not explored in this paper although such processes should result in more ram pressure stripping and therefore a lower final gas mass in all dwarfs.

The disk of the dwarf galaxy is assumed to consist of a cold/warm mixture of gas with an initial hydrogen mass, M_{gas} , equal to the baryon (after accounting for He)/dark matter ratio at $z = 0$ ($M_{\text{gas}} = 0.12 M_{\text{dw},0}$; Komatsu et al. 2011). The disk is chosen to be an exponential disk three scale lengths in size (a reduction in density of 95% and towards the limit that the disk of dwarf galaxies have been seen to continue out to Hunter et al. 2011), with the scale length of the gas assumed to be proportional to the scale length of the optical disk (Bigiel & Blitz 2012). The scale length of the disk, R_{sd} , is then approximately given by (Bigiel & Blitz 2012)

$$R_{\text{sd}} = 0.61 \left(\frac{M_{\text{gas}}}{172 M_{\odot}} \right)^{1/2} \text{ pc}. \quad (3)$$

The exponential profile of the disk then gives a surface density

$$\Sigma_{\text{gas}}(R) = \frac{M_d}{2\pi R_{sd}^2} \exp(-R/R_{sd}), \quad (4)$$

where M_d is related to $M_{\text{disk}} = M_{\text{gas}} + M_{\text{hot}}$ through

$$M_d = \frac{M_{\text{disk}}}{R_{sd}} (R_{sd} - [R_d + R_{sd}] \exp[-R_d/R_{sd}]), \quad (5)$$

where R_d is the radial size of the disk (initially $R_d = 3R_{sd}$). We also assume that initially there is a negligibly small hot halo of the dwarf and therefore $M_{\text{disk}} = M_{\text{gas}}$.

The disk is initially assumed to be split equally between a cold gas phase and warm gas phase (therefore, $X_c = 0.5$ initially) with respective temperatures of $T_c = 400$ K and $T_w = 1.2 \times 10^4$ K. The central density of cold gas is assumed to be $n_c = 1.5 \text{ cm}^{-3}$ in line with the observed densities in Leo T (Ryan-Weber et al. 2008; Greivich & Putman 2009) and the density of warm gas to be $n_w = \frac{1}{2} \frac{T_c}{T_w} \sim 0.17 \text{ cm}^{-3}$.

The size of the hot halo is assumed to be initially small (but non-zero for numerical reasons) and is set to be $R_h = 0.01$ kpc. The temperature of any hot halo that forms is assumed to be constant at 1×10^6 K with a central density of $n_h = \frac{1}{2} \frac{T_c}{T_h} \sim 2 \times 10^{-4} \text{ cm}^{-3}$.

2.3. Heating and Cooling

The disk of a dwarf galaxy is unlikely to experience a steady balance of heating and cooling. Being of low mass without densities large enough to guarantee self-shielding such dwarfs will experience a variety of heating processes throughout their lifetime. The most powerful of these heating processes consist of the host galaxy radiation field, the extragalactic UV field and the dwarfs own internal star formation.

The host galaxy radiation field and the extragalactic UV field are modelled as in NBH, i.e. a host galaxy emitting (after correcting for the escape fraction) 2.6×10^{51} photons s^{-1} at 13.6 eV (Bland-Hawthorn & Maloney 1999) scaled according to star formation history of the Milky Way given by Just & Jahreiß (2010) and an extragalactic radiation field given by Faucher-Giguère et al. (2009).

The internal star formation in the dwarfs disk is given by the Kennicutt-Schmidt law. Although the typical threshold of star formation is $M_{\text{HI}} \sim 10^{21} \text{ cm}^{-3}$ inside larger galaxies, there is little indication that such a threshold is present inside all dwarf galaxies (Roychowdhury et al. 2009). We choose a threshold of $N_{\text{HI}} = 10^{20} \text{ cm}^{-2}$ for the main model and discuss the impact of varying thresholds in §3.1.

The impact of the star formation and extragalactic UV field is precalculated for a range of disk sizes, redshifts and column densities considering only H and He using the prescription of Wolfire et al. (1995). The results are interpolated from this table inside the model in order to reduce the computational time. The cooling is also precomputed assuming metal line cooling at a metallicity of $0.1 Z_{\odot}$ with the fits provided by Schure et al. (2009) and He collisional cooling accounted for according to Dalgarno & McCray (1972). The cooling is assumed to happen equally over the entire disk, with the disk

height assumed to be constant across the disk with the density of gas changing radially in line with the surface density.

These processes result only in a change to X_c according to

$$\dot{X}_c = \frac{\dot{M}_{\text{cool}} - \dot{M}_{\text{heat}}}{M_{\text{disk}}}. \quad (6)$$

In addition to ionizing and heating cold gas the star formation also induces galactic winds from radiation pressure, supernovae and stellar winds. Inside dwarf galaxies the latter two cases are likely to be dominant (Hopkins et al. 2012). To model these winds we extend the fitting formula from Hopkins et al. (2012) down to the dwarf galaxy scales considered here, with the magnitude of mass loss given by

$$\dot{M}_{\text{wind}} = 10 \text{ SFR } V_{\text{circ},100}^{-1.1}(r) \Sigma_{\text{HI},10}^{-0.6}(r) M_{\odot} \text{ yr}^{-1}, \quad (7)$$

where SFR is the star formation rate, $V_{\text{circ},100}$ is the circular velocity of the dwarf in units of 100 km s^{-1} and $\Sigma_{\text{HI},10}$ is the gas density in units of $10 M_{\odot} \text{ pc}^{-2}$ calculated at the wind origin. We assume the wind always launches from the origin and hence may slightly overestimate the magnitude of the wind.

The wind is assumed to lower the height of the disk—that is, takes away mass from the disk while leaving the density of gas constant—while adding to the hot halo. Much of the wind will in reality be entrained material rather than hot gas. Such material may fall back to the disk in a galactic fountain, however, it is likely that the majority will be removed via ram pressure stripping before it has a chance to fall back to the disk or it will be destroyed through conduction in the dwarfs hot halo. Such a wind therefore induces a change in M_d and R_h of

$$\dot{M}_d = -\dot{M}_{\text{wind}} \frac{R_{sd}}{R_{sd} - (R_d + R_{sd}) \exp(-R_d/R_{sd})} \quad (8)$$

$$\dot{R}_{h,\text{IRPS}} = \frac{\dot{M}_{\text{wind}}}{4\pi R_h m_{\text{H}} n_h} f_{\text{gas}}(R_h/R_{s,dw}, v_{s,dw}), \quad (9)$$

where $\dot{R}_{h,\text{IRPS}}$ is the change in the dwarfs halo radius, not accounting for ram pressure stripping; $f_{\text{gas}}(x, v_s)$ is the hydrostatic gas distribution for an Einasto halo (see Sternberg et al. 2002; Nichols & Bland-Hawthorn 2009); $R_{s,dw}$ is the scale radius of the dwarf's dark matter halo and; $v_{s,dw}$ is the scale velocity of the dwarf's dark matter halo.

2.4. Ram Pressure Stripping

As the dwarf is moving relative to the host galaxy hot halo, it will experience a ram pressure force acting upon both its disk and the hot halo. We model the hot halo of the host galaxy by assuming it follows an exponential profile of form $\rho_{\text{gal}} \propto \exp[-V/c_s^2]$ where, V is the potential of the host galaxy at the dwarfs point and c_s is the speed of sound inside the hot halo (assumed to be comprised of a primordial mixture of H and He with a temperature of 2×10^6 K). The factor of proportionality is determined by setting a Milky Way sized host galaxy to have a number density of $3 \times 10^{-4} \text{ cm}^{-3}$ at a distance of 50 kpc. Such a value is consistent with calculations of Battaglia et al. (2005), Bland-Hawthorn et al. (2007) and Kaufmann et al. (2009).

To calculate ram pressure stripping the hydrostatic halo of the dwarf is approximated as an isothermal sphere, with the ram pressure condition (S_{RPS}) for the hot halo then being (McCarthy et al. 2008)

$$S_{\text{RPS,h}}\rho_{\text{gal}}(r)v^2 - \frac{\pi}{2} \frac{GM_{dw}(R_h)\rho_{\text{halo}}(R_h)}{R_h} > 0, \quad (10)$$

where $v^2 = \dot{r}^2 + (r\dot{\theta})^2$, $M_{dw}(R_h)$ is the mass of the dwarf enclosed within the dwarf's hot halo outer edge, $\rho_{\text{halo}}(R_h)$ is the density of the dwarf's hot halo at this edge and ram pressure stripping occurs if S_h evaluates true. We ignore any potential hydrodynamic interaction between the disk and the halo which may have a minor protective effect (Bekki 2009).

The disk is assumed to be protected from ram pressure stripping until the dwarf's hot halo is reduced beyond the borders of the disk (i.e. ram pressure stripping only occurs if $R_d > R_h$ although this condition is nearly always satisfied when the disk would be stripped). If this is true, the condition for ram pressure stripping is then given by (McCarthy et al. 2008)

$$S_{\text{RPS,d}} = \rho_{\text{gal}}(r)v^2 - g_{\text{max}}(R_d)\Sigma_{\text{disk}}(R_d) > 0, \quad (11)$$

where $g_{\text{max}}(R_d)$ is the maximum restoring force of the gas in the direction of v and Σ is the projected gas density. For simplicity we assume that the disk is moving face on, although there is little difference for a wide range of angles (Quilis et al. 2000; Jáchym et al. 2009). For an Einasto halo with $\alpha = 0.16$, $g_{\text{max}}(R_d)$ is well fit (to at least a few dwarf scale radius) by

$$g_{\text{max}}(R_d) = \frac{6.63 \times 10^{-4} v_{s,dw}^2}{R_{s,dw}} 10^{15-1.03(R_d/R_{s,dw})^{0.41}}. \quad (12)$$

If the disk has expanded past the point of maximum gravitational attraction, h_{max} , the value of g_{max} is weighted by calculating the average value of the gravitational attraction (with all mass below h_{max} assumed to have g_{max} attraction). h_{max} is well fit by

$$h_{\text{max}} = \sqrt{2.11 \left(\frac{R_d}{R_{s,dw}} \right)^{0.137} R_{s,dw}^2 - R_d^2}. \quad (13)$$

If either the dwarf's hot halo or disk experience ram pressure stripping the radius is reduced in proportion to the speed of shock induced (Mori & Burkert 2000)

$$v_{\text{shock}} = \frac{4}{3}v \sqrt{\frac{\rho_{\text{gal}}}{\rho_{\text{halo/disk}}}}. \quad (14)$$

For simplicity we assume the gas is removed in shells and hence the change in radius due to this removal is half of v_{shock} . We also tested a different rate of ram pressure stripping $v_{\text{shock}} \sim (2/3)c_s$ from McCarthy et al. (2008) but found minimal variation in the final results.

The rate of change of the radius and hot halo can therefore be written as

$$\dot{R}_h = \dot{R}_{h,\text{!RPS}} - 0.5v_{\text{shock}}S_{\text{RPS,h}}, \quad (15)$$

$$\dot{R}_d = -0.5v_{\text{shock}}S_{\text{RPS,d}}(R_d > R_h), \quad (16)$$

where all Boolean values are calculated as integers in the standard way, 1 if true and 0 if false.

3. RESULTS

The model was run for varying virial masses of $M_{\text{vir}} = 3 \times 10^8, 1 \times 10^9, 3 \times 10^9, 1 \times 10^{10}, 3 \times 10^{10}$ and $1 \times 10^{11} M_{\odot}$ in two halos of $z = 0$ virial mass $1.37 \times 10^{12} M_{\odot}$ (consistent with the circular velocity of the RAVE survey; Smith et al. 2007) and $2 \times 10^{12} M_{\odot}$. We note that under the chosen model of growth (where dwarfs do not undergo mergers or growth), the larger dwarfs may initially be more massive than the host galaxy (which does experience growth), we ignore any effects this may have on the model although note that it may impact the earliest redshifts.

Figure 1 shows the effect of final perigalacticon and circularity of the dwarf on the amount of HI retained at the present day in a host halo of $M_{\text{vir},0} = 1.37 \times 10^{12} M_{\odot}$. As may be intuitively expected, dwarfs with smaller perigalacticons lose a greater percentage of their initial mass. Dwarfs with a medium circularity, ($\eta \sim 0.5$), seem to lose more mass than those that with larger or smaller circularities. Although such dwarfs spend less time in the denser part of the host halo than those on more circular orbits, the greater speed they obtain at perigalacticon may more than compensate for this. There may be a similar effect at high perigalacticon, low circularity, where the extreme velocities encountered mean any tenuous medium is still able to strip some material from the dwarfs, however, there are very few dwarfs found in these regions and such an effect may just be noise.

For dwarfs in a host halo $\sim 50\%$ larger at $M_{\text{vir},0} = 2 \times 10^{12} M_{\odot}$ the result is much the same and is shown in figure 2, with the only noticeable difference being a possible reduction in the gas mass for low circularity, low perigalacticon orbits. Such a reduction likely occurs where the increased density, combined with the increased orbital speed in the more massive halo manages to strip these dwarfs where the previous host halo could not.

3.1. Star Formation Threshold

Changing the star formation threshold dramatically changes the amount of gas that dwarfs are able to retain. We examine this through a comparison of three threshold levels of HI required in the model for star formation (10^{19} cm^{-2} , 10^{20} cm^{-2} and 10^{21} cm^{-2}).

Dwarfs with a low threshold ($N_{\text{HI}} = 10^{19} \text{ cm}^{-2}$) of star formation produce large amounts of star formation initially and subsequently blow out large amounts of gas through galactic winds. Such an extended hot halo is then easily stripped by any passage through the host halo. Dwarfs with a high threshold ($N_{\text{HI}} = 10^{21} \text{ cm}^{-2}$) experience the opposite problem. Without strong winds forcing gas into a hot halo, the disk retains too much mass to be effectively stripped in all but the densest parts of the host halo. The strength of these effects are shown in figure 3

4. THE LOCAL GROUP AND THE M81 GROUP

We can use this model to obtain an estimate of the accretion time of the Local Group and other galaxy groups. Most dwarf satellites within the Local Group are satellites of the Milky Way or M31. Dwarfs around both galaxies are HI deficient within the virial radius of either (Grcevich & Putman 2009). We previously showed in NBH that such an effect implies that dwarfs begun ac-

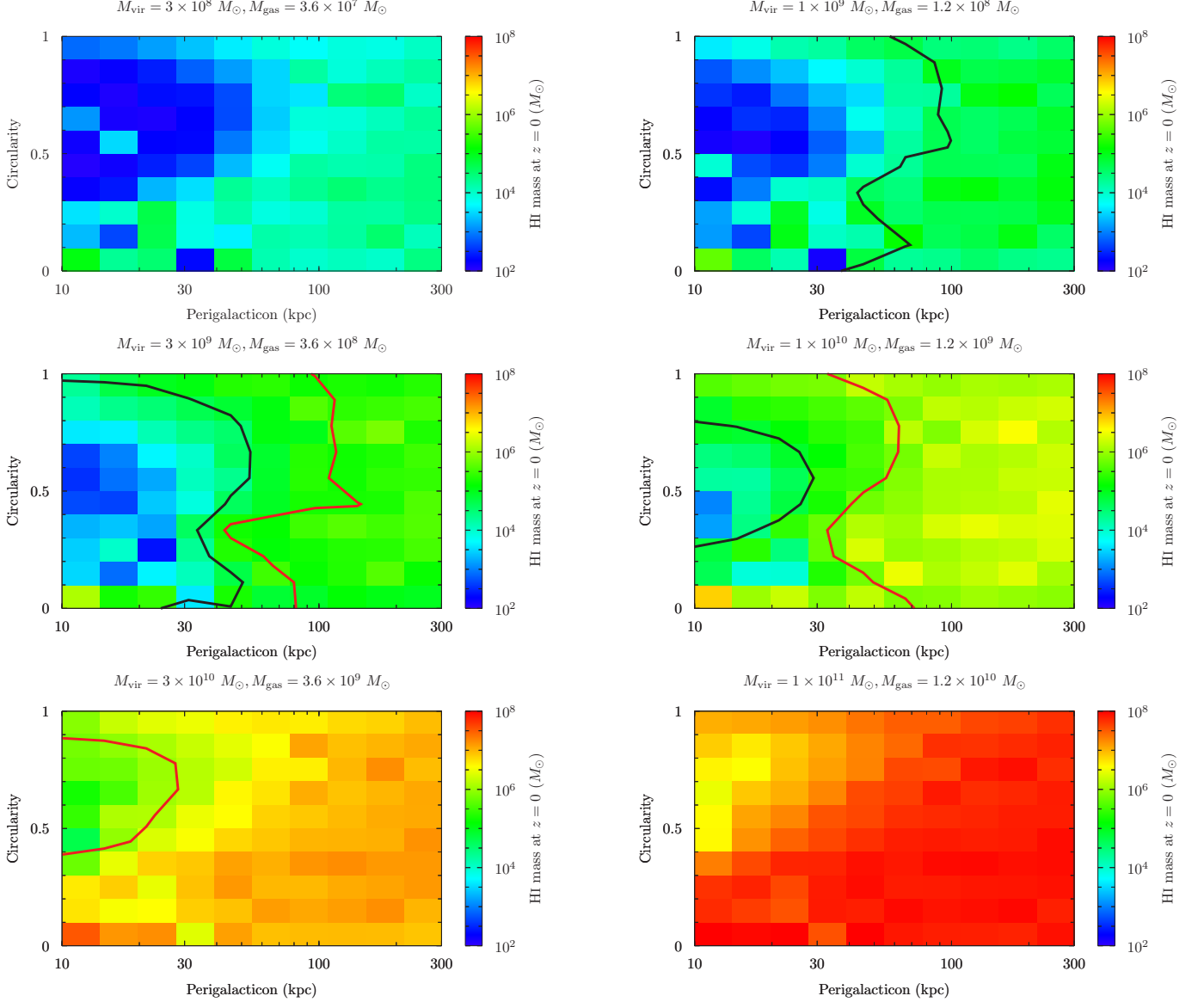


FIG. 1.— The present day HI mass for dwarfs around a host halo with $M_{\text{vir},0} = 1.37 \times 10^{12} M_{\odot}$ (Smith et al. 2007), as a function of present day perigalacticon and circularity. Dwarfs of mass above $M_{\text{dw}} = 1 \times 10^{10} M_{\odot}$ are not shown, as nearly all retain over $10^5 M_{\odot}$ of HI. The gas mass listed is the initial Hydrogen mass at $z = 10$ and is a combination of HI and HII. The color map is constructed using an inverse square interpolation from the randomly generated points. The star formation threshold is $N_{\text{HI}} = 10^{20} \text{ cm}^{-2}$. Contours of the smallest gas mass seen in the Local Group ($M_{\text{HI}} = 10^5 M_{\odot}$) and the M81 group ($M_{\text{HI}} = 10^6 M_{\odot}$) are shown as solid and dashed white (black and red solid) lines respectively. Unless closed, areas to the left are under the relevant gas mass. Even at masses below the SMC and LMC many halos will survive at low galactocentric radius and it is therefore unsurprising that they are as of yet unstripped. (A colored version of this figure is available online.)

creting at an early time ($z = 3-10$). In figure 4 we show the fraction of dwarfs that exceed $1 \times 10^5 M_{\odot}$ of HI at $z = 0$ for the lowest mass dwarfs, defining the accretion time as the first time dwarfs passing through the virial radius of the host halo and including those that never pass through the virial radius in all cutoffs. Compared to NBH, the accretion time suggested for the smallest mass dwarfs is more recent, a product of the strong dwarf winds that are now accounted for.

Using the mass spectrum for dwarfs from Via Lactea II (Diemand et al. 2007) the expected fraction of all satellites can be reproduced and is shown in figure 5. Here, even accretion beginning at redshift of 10 slightly overestimates the final fraction, a possible impact of

the lower stellar mass of the model dwarfs compared to reality. In addition, the Local Group is assumed to be observationally complete (or at least unbiased to mass/galactocentric distance). Such a proposition is unlikely and it is probable that future detections of dwarfs will be the gas-deficient low mass objects as have recently been discovered. Such an overestimate therefore makes it more unlikely that the Milky Way begun accreting later than redshift 10.

Detailed studies of external groups are only just beginning. To allow for a proper comparison, we note that the M81 group survey is complete down to a limiting absolute magnitude of $M_r = -10$ (Chiboucas et al. 2009) and therefore choose this cut-off magnitude for the

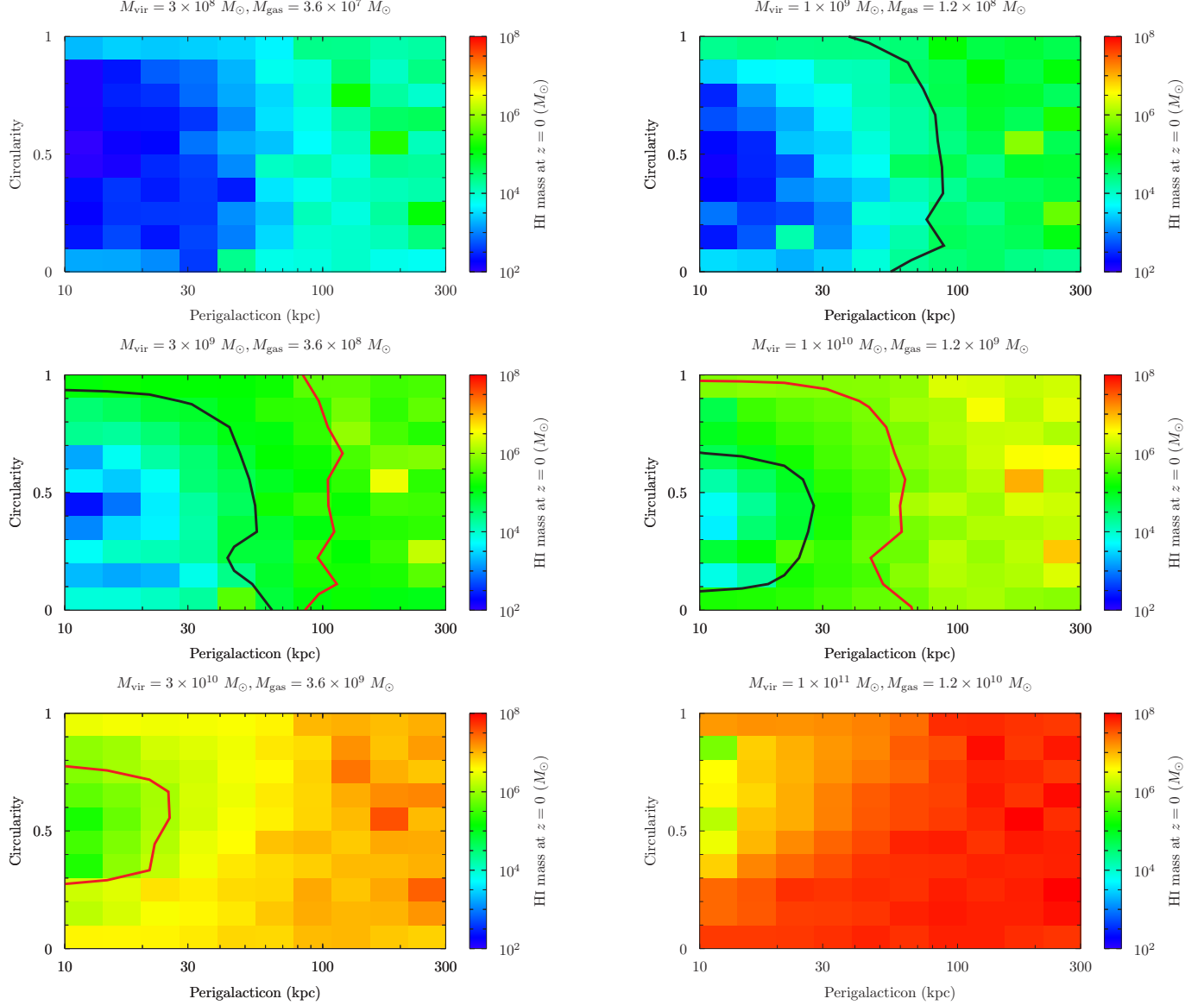


FIG. 2.— The present day HI mass for dwarfs around a host halo with $M_{\text{vir},0} = 2 \times 10^{12} M_{\odot}$, as a function of present day perigalacticon and circularity. The gas mass listed is the initial Hydrogen mass at $z = 10$ and is a combination of HI and HII. The color map is constructed using an inverse square interpolation from the randomly generated points. The star formation threshold is $N_{\text{HI}} = 10^{20} \text{ cm}^{-2}$. Contours of the smallest gas mass seen in the Local Group ($M_{\text{HI}} = 10^5 M_{\odot}$) and the M81 group ($M_{\text{HI}} = 10^6 M_{\odot}$) are shown as solid and dashed white (black and red solid) lines respectively. Unless closed, areas to the left are under the relevant gas mass. (A color version of this figure is available online.)

Local Group. To determine the dwarf mass that satisfies this cut, we examine the integrated star formation over time and use the integrated stellar mass of Sculptor ($M_r = -10.25$; Jerjen et al. 1998) of $\sim 1.2 \times 10^6 M_{\odot}$ (Woo et al. 2008) to approximate this cut-off. The closest model dwarf mass to this lifetime-integrated star formation is that of $M_{\text{dw}} = 3 \times 10^9 M_{\odot}$ and we therefore use it as the cut-off limit. Such a mass is slightly above the common mass scale observed in the Local Group (Strigari et al. 2008) with $M_{\text{dw}} = 3 \times 10^9 M_{\odot}$ corresponding to a mass of $4 \times 10^7 M_{\odot}$ within 300 pc and this difference may reflect an inadequate star formation rate or be a consequence of baryonic processes lowering the central density (and therefore mass within 300 pc).

We display the fraction of galaxies with $M_{\text{HI}} > 10^6 M_{\odot}$ in the model against the M81 group and the

Local Group in figure 6. We use the HI masses from Karachentsev & Kaisin (2007) and Roychowdhury et al. (2012), and the distances from Karachentsev et al. (2002). The threshold is just above the lowest confirmed gas mass (d1014+68 with $7.5 \times 10^5 M_{\odot}$ of HI Roychowdhury et al. 2012) and we assume that dwarfs with only a published upper limit above this threshold fall below it. We bin the results into 100 kpc bins to smooth out the rapid changes that occur due to the small number of dwarfs involved. Here the Local Group is satisfied by galaxies that begun accreting at redshift $z \sim 3-10$, while the M81 Group is best fit by a later accretion epoch ($z = 1-3$). Within a few virial radii (where low number statistics may be more prevalent, but without any potential errors from association with the wrong host), M81 is best fit by accretion at approximately $z \sim 1$

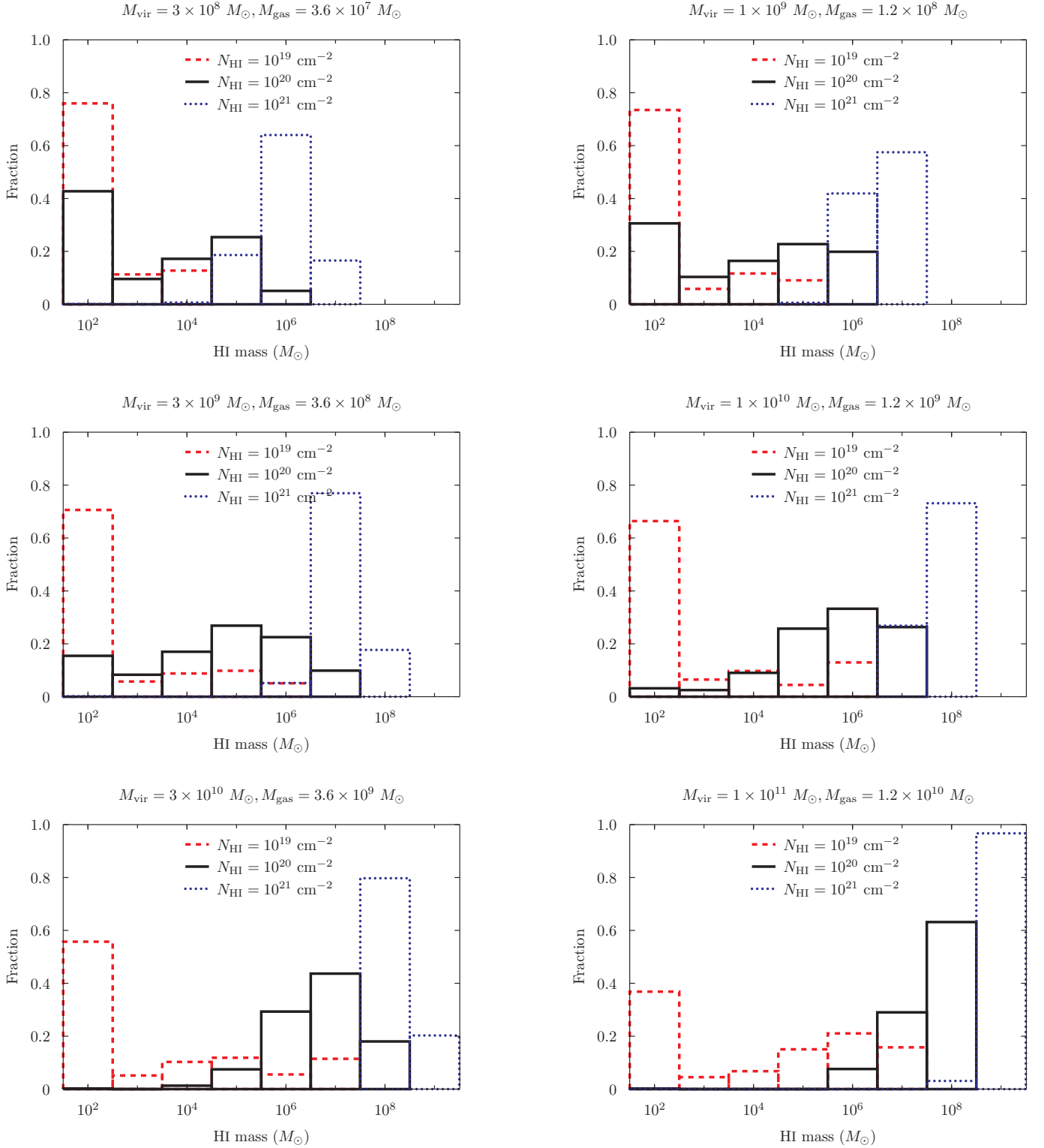


FIG. 3.— Histogram of HI retained in dwarf galaxies with varying star formation thresholds. A cutoff of 10^{19} cm^{-2} is shown as a (red) dashed line, 10^{20} cm^{-2} as a black solid line and 10^{21} cm^{-2} is shown as a (blue) dotted line. The amount of HI is displayed logarithmically with any gas mass below $10^2 M_{\odot}$ being included in that bin. The host halo was assumed to be a Milky Way like halo with a virial mass of $M_{\text{vir},0} = 1.37 \times 10^{12} M_{\odot}$. (A colored version of this figure is available online.)

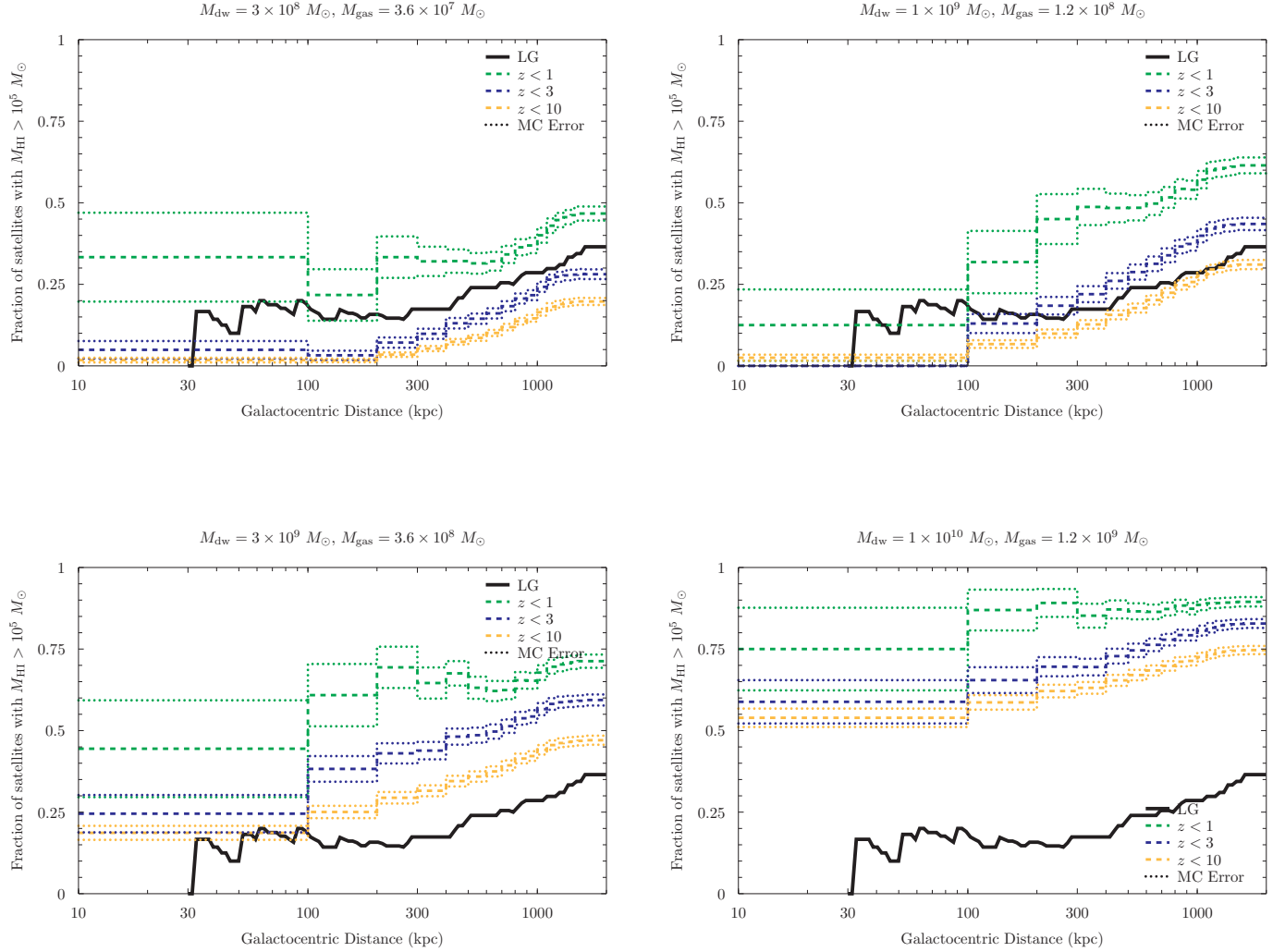


FIG. 4.— Fraction of dwarf galaxies below a radius that contains over $10^5 M_\odot$ of HI when orbiting a host galaxy of mass $M_{\text{vir},0} = 1.37 \times 10^{12} M_\odot$. The data for the Local Group is from Grevesch & Putman (2009). The accretion time is given by the time the dwarf first passed through the virial radius of the halo, with dwarfs that never do so being included in each. Dwarfs that accreted after redshift 1 (or never) are shown with a dashed (green dashed) line, dwarfs which accreted after redshift 3 (or never) are shown with a dot-dash (blue dashed) line and those which accreted after redshift 10 (or never) are shown with a long-dashed (yellow dashed) line. For clarity, we have binned the results into 100 kpc bins with the resulting lines representing the end point of each bin (i.e. 100–200 kpc gives the value at 200 kpc). In each case at high galactocentric distances dwarfs which accrete later have a higher fraction of gas that survives. At low galactocentric radius this is not necessarily true where low number statistics dominates. An estimate of the error given by the standard deviation of each dwarf from the line divided by the number of dwarfs is shown as dashed lines in the same color. (A colored version of this figure is available online.)

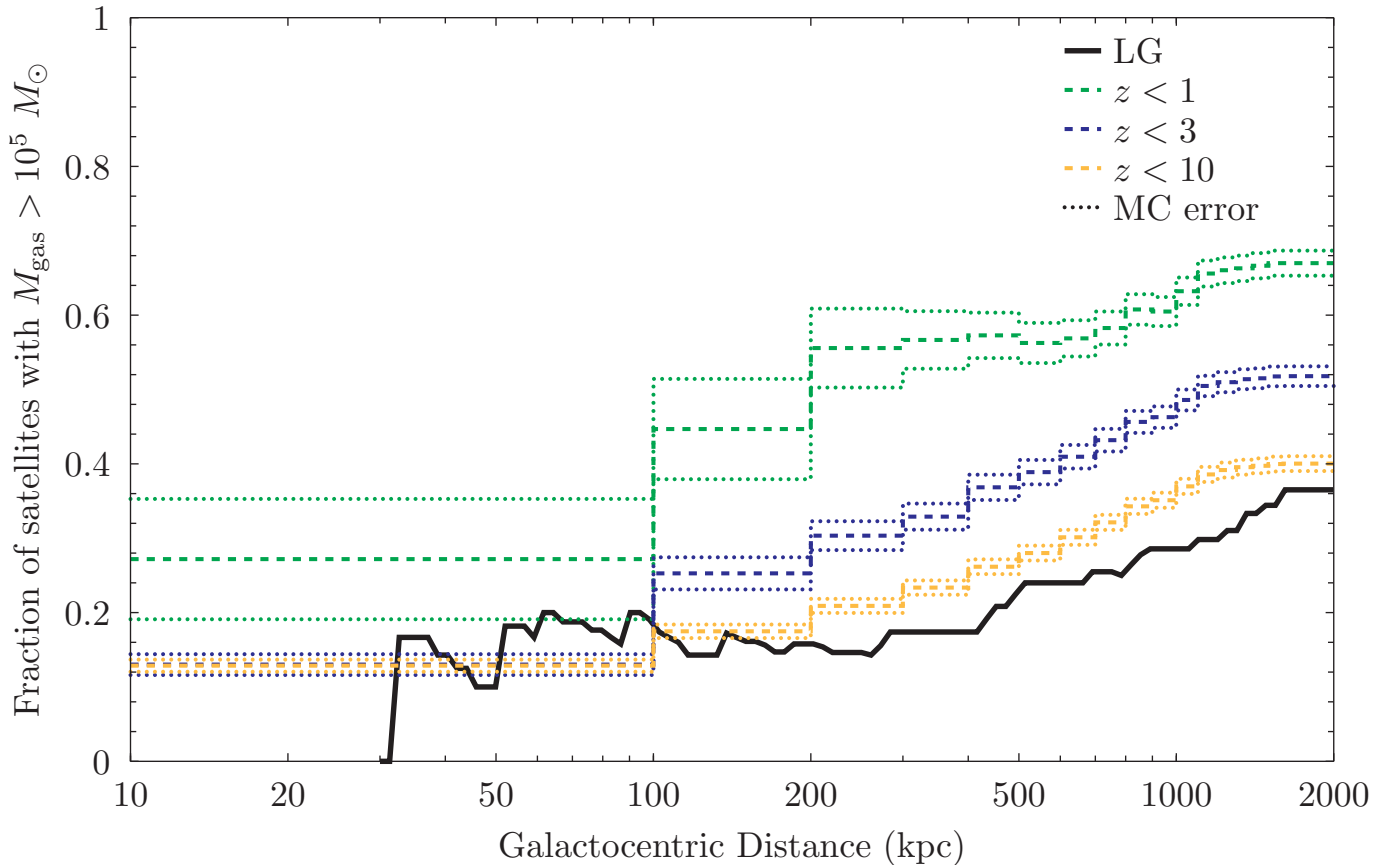


FIG. 5.— Fraction of dwarf galaxies below a radius that contain over $10^5 M_\odot$ of HI weighted according to the mass spectrum of dwarfs in Via Lactea II (Diemand et al. 2007). The redshift cutoffs are the same as figure 4.

and the Local Group by $z \sim 10$.

If the initial gas mass is limited by the dwarfs mass at $z = z_{\text{acc}}$ ($M_{\text{gas}} = 0.12 M_{\text{dw,acc}}$), the accretion time of the LG drops slightly, becoming closer to $z = 3$ than $z = 10$. In this scenario, figure 7, both the Local Group and the M81 group require slightly more recent accretion. The difference is slight however, as a large number of dwarf galaxies never pass the virial radius of the host galaxy.

5. CONCLUSION

The model presented is able to reproduce the observed fraction of gas-rich satellite dwarfs around a host halo. Such a model is able to differentiate between accretion times between two galaxy groups and suggests that the satellites around the M81 group accreted at a later time. Assuming that dwarf galaxies begun with a gas mass sufficient to give them the cosmic fraction of baryons to dark matter today if no gas had been lost suggests that the accretion of satellites by the largest galaxies in the Local Group (the Milky Way and M31) begun at an early redshift $z \sim 10$. Applying a magnitude cut-off to examine only the more massive dwarf galaxies suggests that they begun accreting at a similar time in the Local Group and that similar dwarfs inside the M81 group begun accreting more recently $z \sim 1 - 3$ and hence the M81 group started accreting its satellite galaxies ~ 2 Gyr later than the Local Group. Such a result may also be reflected in the masses of the HVC population with many large HI clouds (with cloud masses up to $8 \times 10^7 M_\odot$; Chynoweth et al. 2011) compared to the Local Group (with a total HVC

mass $\sim 10^8 M_\odot$; Lehner et al. 2012).

Such a model although informative still has significant limitations when run on desktop machines. Extending this model to Markov chain Monte Carlo algorithms is being investigated to remove or minimize some of these limitations. The metallicity is assumed constant at a metallicity approximately that observed today in the most massive dwarfs (Mateo 1998), such an assumption will lead to overcooling at the highest redshifts and in the smaller dwarfs and hence may be indicative of a later accretion time. Acting in a similar way is the assumption of the initial gas mass, it is unlikely that the shallow potential well of a dwarf is able to gather such quantities of gas at high redshift, and the exact amount may vary on the accretion time of the dwarf. The amount of gas initially should therefore be considered an upper limit, suggesting again a more recent accretion time than the model predicts. The model also ignores the possibility of future low-redshift accretion or reaccretion of gas by dwarfs (a distinct possibility, see Ricotti 2009; Nichols et al. 2012), findings of significant gas accretion by satellites would be indicative of higher redshift accretion. The dark matter potential of the dwarf is also assumed to be constant, a central density reduction in the dwarf will likely lead to gas being more easily removed from the centre and be indicative again of a more recent accretion time. The gas distribution is assumed smooth, however, fractal distributions (more representative of the clumpy nature of dwarf disks) leads to faster stripping as instabilities build up which would require

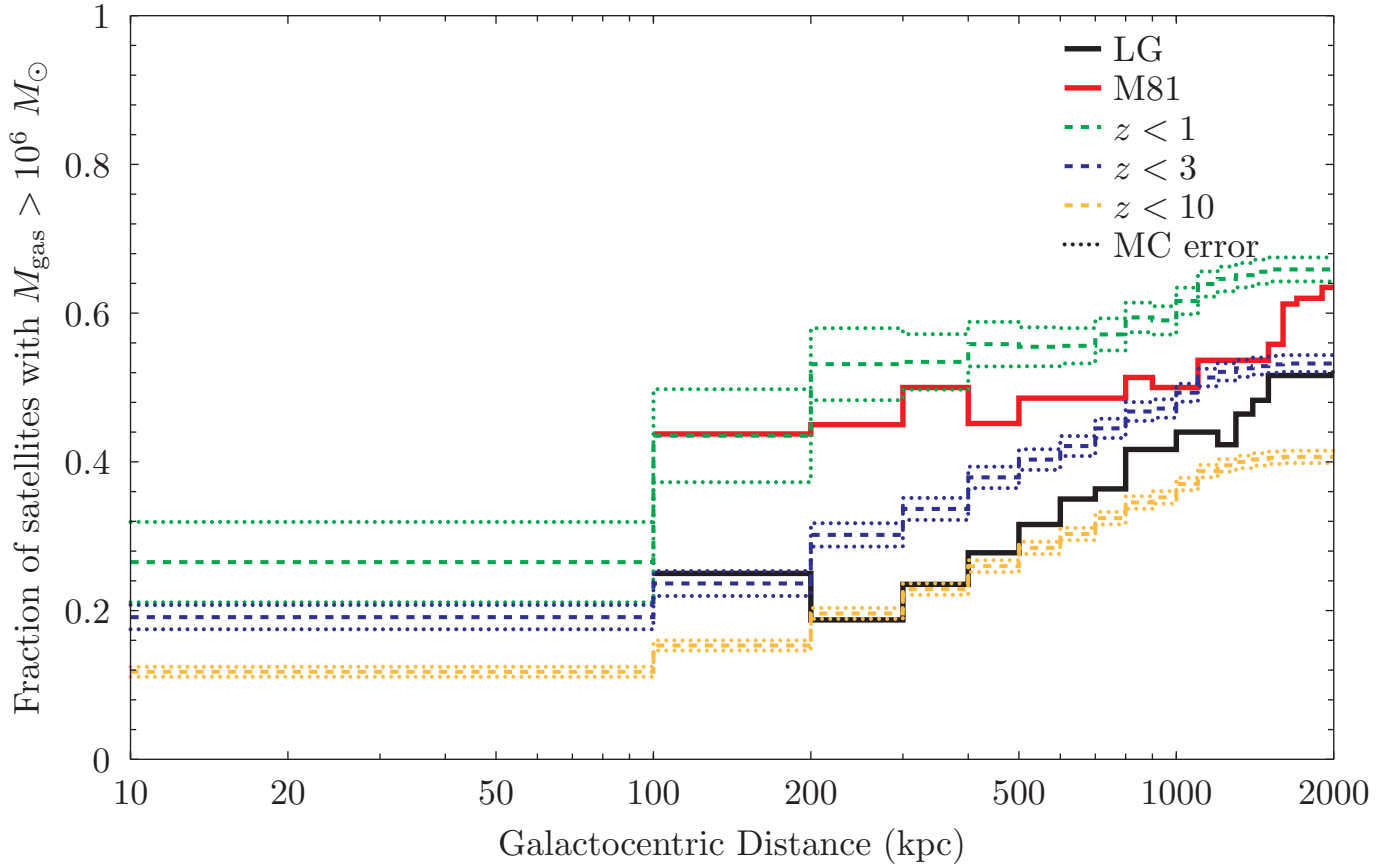


FIG. 6.— Fraction of dwarf galaxies below a given radius that contain over $10^6 M_{\odot}$ of HI. The fraction of observed galaxies that contain this in the Local Group is shown as a (black) solid line and the fraction in the M81 group shown as a (red solid) long-short dashed line. Only galaxies brighter than Sculptor are included. We bin these observed galaxies into 100 kpc bins to reduce rapid changes in fractions due to the low number of galaxies involved. The model cut-offs are shown as dashed, dash-dot, long-dashed (dashed green, blue and yellow) lines as in figure 4, with the binning of results the same. Below ~ 100 kpc the groups are dominated by small number statistics, we subsequently leave this first bin off. (A color version of this figure is available online.)

dwarfs to have been accreted more recently to produce the same distribution. Furthermore, we have neglected tidal forces within this model. As tidal forces decrease gas density at perigalacticon (where they are strongest) and as ram pressure stripping experiences a maximum at this same point, synergistic effects are possible. Furthermore, we ignore some regions where tidal forces may be able to remove gas without the need for ram pressure stripping through synergistic effects between tides and supernova (Nichols et al. 2013). The accuracy of the analytic approximations will be compared with upcoming hydrodynamical simulations to allow for future calibration of this model.

Taken together it is likely that dwarfs accrete more recently than this model suggests but as these should happen in similar ways for all galaxy groups, such a model can be used to quickly determine an approximation of

accretion time of a galaxy group and provides further evidence that even the local universe shows large differences in the accretion histories of nearby groups.

The dwarf model presented here may be refined further as proper motion measurements of dwarfs inside the Local Group improve, assisting the determination of accretion time (Rocha et al. 2012). Such an improvement in proper motions seems unlikely for external groups. Future multi-wavelength observations of the Local Group and external groups may also assist in the refinement of this model through narrowing of the allowed parameter space. In particular, further observations of nearby groups (e.g. Chynoweth et al. 2011) will allow the extension of this model to more clusters, allowing a comprehensive study of the accretion of the nearby universe.

JBH is funded by a Federation Fellowship from the Australian Research Council.

REFERENCES

- Bahé, Y. M., McCarthy, I. G., Balogh, M. L., & Font, A. S. 2013, MNRAS, 430, 3017
 Barkana, R., & Loeb, A. 1999, ApJ, 523, 54
 Battaglia, G., Helmi, A., Morrison, H., et al. 2005, MNRAS, 364, 433
 Bekki, K. 2009, MNRAS, 399, 2221
 —. 2011, MNRAS, 416, 2359
 Besla, G., Kallivayalil, N., Hernquist, L., et al. 2007, ApJ, 668, 949
 Bigiel, F., & Blitz, L. 2012, ApJ, 756, 183
 Bland-Hawthorn, J., & Maloney, P. R. 1999, ApJ, 510, L33
 Bland-Hawthorn, J., Sutherland, R., Agertz, O., & Moore, B. 2007, ApJ, 670, L109
 Bode, P., Ostriker, J. P., & Turok, N. 2001, ApJ, 556, 93

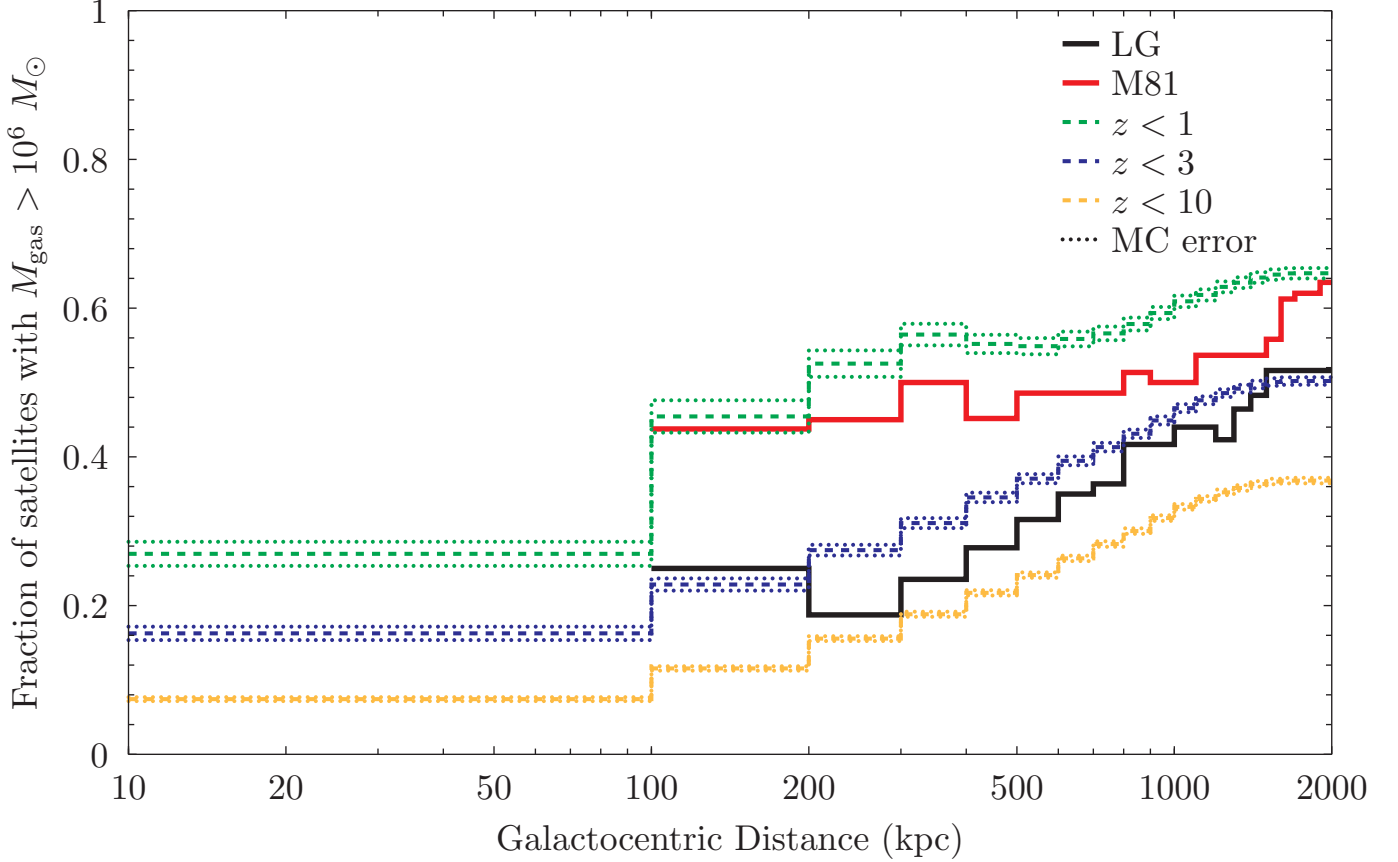


FIG. 7.— Fraction of dwarf galaxies below a given radius that contain over $10^6 M_{\odot}$ of HI. The fraction of observed galaxies that contain this in the Local Group is shown as a (black) solid line and the fraction in the M81 group shown as a long-short dashed (red solid) line. The model cut-offs are shown as dashed, dash-dot and long-dashed (dashed green, blue and yellow) lines as in fig 4, with the binning of results the same. Below ~ 100 kpc the groups are dominated by small number statistics, we subsequently leave this first bin off. The initial gas mass is set by $M_{\text{gas}} = 0.12 M_{\text{dw,acc}}$ in contrast to figure 6. (A color version of this figure is available online.)

Boylan-Kolchin, M., Springel, V., White, S. D. M., & Jenkins, A. 2010, *MNRAS*, 406, 896
 Chiboucas, K., Jacobs, B. A., Tully, R. B., & Karachentsev, I. D. 2013, *AJ* submitted
 Chiboucas, K., Karachentsev, I. D., & Tully, R. B. 2009, *AJ*, 137, 3009
 Chynoweth, K. M., Langston, G. I., & Holley-Bockelmann, K. 2011, *AJ*, 141, 9
 Colín, P., Klypin, A., Valenzuela, O., & Gottlöber, S. 2004, *ApJ*, 612, 50
 Crnojević, D., Grebel, E. K., & Cole, A. A. 2012, *A&A*, 541, A131
 Dalgarno, A., & McCray, R. A. 1972, *ARA&A*, 10, 375
 de Blok, W. J. G., & Walter, F. 2006, *AJ*, 131, 363
 Del Popolo, A. 2012, *MNRAS*, 419, 971
 Diemand, J., Kuhlen, M., & Madau, P. 2007, *ApJ*, 657, 262
 D’Onghia, E., Besla, G., Cox, T. J., & Hernquist, L. 2009, *Nature*, 460, 605
 Duffy, A. R., Schaye, J., Kay, S. T., & Dalla Vecchia, C. 2008, *MNRAS*, 390, L64
 Ekta, Chengalur, J. N., & Pustilnik, S. A. 2008, *MNRAS*, 391, 881
 Faucher-Giguère, C., Lidz, A., Zaldarriaga, M., & Hernquist, L. 2009, *ApJ*, 703, 1416
 Grebel, A., & Bromm, V. 2012, *ApJ*, 759, 115
 Grebel, A., Kirby, E. N., & Simon, J. D. 2010, *Nature*, 464, 72
 Gao, L., Navarro, J. F., Cole, S., et al. 2008, *MNRAS*, 387, 536
 Greivich, J., & Putman, M. E. 2009, *ApJ*, 696, 385
 Grebel, E. K., Gallagher, III, J. S., & Harbeck, D. 2003, *AJ*, 125, 1926
 Helmi, A., Sales, L. V., Starkenburg, E., et al. 2012, *ApJ*, 758, L5
 Hoeft, M., Yepes, G., Gottlöber, S., & Springel, V. 2006, *MNRAS*, 371, 401
 Hopkins, P. F., Quataert, E., & Murray, N. 2012, *MNRAS*, 421, 3522
 Hunter, D. A., Elmegreen, B. G., Oh, S.-H., et al. 2011, *AJ*, 142, 121

Jáchym, P., Köppen, J., Palouš, J., & Combes, F. 2009, *A&A*, 500, 693
 Jerjen, H., Freeman, K. C., & Binggeli, B. 1998, *AJ*, 116, 2873
 Just, A., & Jahreiß, H. 2010, *MNRAS*, 402, 461
 Karachentsev, I. D., & Kaisin, S. S. 2007, *AJ*, 133, 1883
 Karachentsev, I. D., Dolphin, A. E., Geisler, D., et al. 2002, *A&A*, 383, 125
 Karlsson, T., Bland-Hawthorn, J., Freeman, K. C., & Silk, J. 2012, *ApJ*, 759, 111
 Karlsson, T., Bromm, V., & Bland-Hawthorn, J. 2013, *Reviews of Modern Physics*, 85, 809
 Kaufmann, T., Bullock, J. S., Maller, A. H., Fang, T., & Wadsley, J. 2009, *MNRAS*, 396, 191
 Komatsu, E., Smith, K. M., Dunkley, J., et al. 2011, *ApJS*, 192, 18
 Kuhlen, M., Krumholz, M. R., Madau, P., Smith, B. D., & Wise, J. 2012, *ApJ*, 749, 36
 Lehner, N., Howk, J. C., Thom, C., et al. 2012, *MNRAS*, 424, 2896
 Lovell, M. R., Eke, V., Frenk, C. S., et al. 2012, *MNRAS*, 420, 2318
 Lunnan, R., Vogelsberger, M., Frebel, A., et al. 2012, *ApJ*, 746, 109
 Lux, H., Read, J. I., & Lake, G. 2010, *MNRAS*, 406, 2312
 Macciò, A. V., & Fontanot, F. 2010, *MNRAS*, 404, L16
 Mateo, M. L. 1998, *ARA&A*, 36, 435
 Mayer, L., Governato, F., Colpi, M., et al. 2001, *ApJ*, 547, L123
 McBride, J., Fakhouri, O., & Ma, C. 2009, *MNRAS*, 398, 1858
 McCarthy, I. G., Frenk, C. S., Font, A. S., et al. 2008, *MNRAS*, 383, 593
 Moore, B., Ghigna, S., Governato, F., et al. 1999, *ApJ*, 524, L19
 Mori, M., & Burkert, A. 2000, *ApJ*, 538, 559
 Nichols, M., & Bland-Hawthorn, J. 2009, *ApJ*, 707, 1642
 —. 2011, *ApJ*, 732, 17
 Nichols, M., Colless, J., Colless, M., & Bland-Hawthorn, J. 2011, *ApJ*, 742, 110
 Nichols, M., Lin, D., & Bland-Hawthorn, J. 2012, *ApJ*, 748, 149

- Nichols, M., Revaz, Y., & Jablonka, P. 2013, in prep.
- Pasetto, S., Chiosi, C., & Carraro, G. 2003, *A&A*, 405, 931
- Pontzen, A., & Governato, F. 2012, *MNRAS*, 421, 3464
- Quilis, V., Moore, B., & Bower, R. 2000, *Science*, 288, 1617
- Rasmussen, J., Bai, X.-N., Mulchaey, J. S., et al. 2012, *ApJ*, 747, 31
- Ricotti, M. 2009, *MNRAS*, 392, L45
- Ricotti, M., Gnedin, N. Y., & Shull, J. M. 2008, *ApJ*, 685, 21
- Rocha, M., Peter, A. H. G., & Bullock, J. 2012, *MNRAS*, 425, 231
- Roychowdhury, S., Chengalur, J. N., Begum, A., & Karachentsev, I. D. 2009, *MNRAS*, 397, 1435
- Roychowdhury, S., Chengalur, J. N., Chiboucas, K., et al. 2012, *MNRAS*, 426, 665
- Ryan-Weber, E. V., Begum, A., Oosterloo, T., et al. 2008, *MNRAS*, 384, 535
- Sawala, T., Scannapieco, C., & White, S. 2012, *MNRAS*, 420, 1714
- Schure, K. M., Kosenko, D., Kaastra, J. S., Keppens, R., & Vink, J. 2009, *A&A*, 508, 751
- Simon, J. D., Bolatto, A. D., Leroy, A., Blitz, L., & Gates, E. L. 2005, *ApJ*, 621, 757
- Smith, M. C., Ruchti, G. R., Helmi, A., et al. 2007, *MNRAS*, 379, 755
- Somerville, R. S. 2002, *ApJ*, 572, L23
- Springel, V., Wang, J., Vogelsberger, M., et al. 2008, *MNRAS*, 391, 1685
- Sternberg, A., McKee, C. F., & Wolfire, M. G. 2002, *ApJS*, 143, 419
- Strigari, L. E., Bullock, J. S., Kaplinghat, M., et al. 2008, *Nature*, 454, 1096
- Teyssier, M., Johnston, K. V., & Kuhlen, M. 2012, *MNRAS*, 426, 1808
- Tolstoy, E. 2011, *Science*, 333, 176
- Wetzel, A. R. 2011, *MNRAS*, 412, 49
- Wolf, J., & Bullock, J. S. 2012, *MNRAS* submitted, arXiv:1203.4240
- Wolfire, M. G., Hollenbach, D., McKee, C. F., Tielens, A. G. G. M., & Bakes, E. L. O. 1995, *ApJ*, 443, 152
- Woo, J., Courteau, S., & Dekel, A. 2008, *MNRAS*, 390, 1453